Quench and stability of Roebel cables at 77 K and self-field: minimum quench power, cold end cooling, and cable cooling efficiency

C J Kovacs, M Majoros, M D Sumption, and E W Collings

The Ohio State University, Columbus, Ohio USA

E-mail: kovacs.34@osu.edu

Abstract. A 9-tape, 14 mm wide ReBCO Roebel cable was soldered onto a U-shaped holder. The critical current, I_c, was measured at 77 K and self-field. The cryostability of the cable was studied in response to the application of local pulses of 1 to 14 W at several values of $i = I/I_c$. A detailed analysis of the cable's cryostability was presented. With a Stekly parameter $\alpha = G/Q \ll 1$ and a heat generation margin of ~190 kW/m^2 the present ReBCO cable was shown to be ultra cryostable with respect to internally generated transport-current overload. However, the cable was much less stable against externally and locally applied disturbances because of the tendency to initiate local film boiling. A locally applied 10 W led to a prediction of a film-boiling-cooled zone with a temperature of 181 K. However, when cold-end cooling was considered, the predicted hot spot temperature decreased to 87-115 K depending on the surface-cooling efficiency. Predictions were compared to experiment extracting a cooling efficiency parameter representing the penetration of the cryogen into the cable. Experiment showed the generation of time stable normal zones which were a function of disturbance power. This led to the description of the cable stability in terms of minimum quench power; the results are presented in stability diagrams.

1. Introduction

High B_{irr} High Temperature Superconductors (HTS) have a number of potential uses, including power, transportation and other (e.g., high field MRI and NMR) applications. An ambitious application is using HTS conductors for next-generation high energy and luminosity colliders. HTS is already being considered for insert coils within the Future Circular Collider's high field dipole magnets [1,2]. Numerous high-field magnets and insert magnets have been demonstrated using HTS conductors and a few high-field HTS-hybrid research magnets are nearly complete for user facilities [3-6]. Bi:2212 cables will likely require a high-pressure, atmospherically-controlled, wind-and-react, and epoxy impregnated magnet manufacturing process while Rare-Earth Barium Copper Oxide (ReBCO) will be react-and-wind, have simpler insulation options, and may not require epoxy impregnation depending on the stresses and cable type [7-10]. The structure of Bi:2212 Rutherford cable is similar to the NbTi and Nb_3Sn Rutherford cables that are presently used, but ReBCO cables are quite different. A comparison of ReBCO Conductor on Round Core (CORC), Twisted-Stack, and Roebel cable designs reveals differences in engineering current density, inductance, and minimum bending radius [1,10]. Roebel cables are created by stamping or cutting ReBCO tape to specially shaped strands [11]. Using special machines, the strands are wound into Roebel cable. One key issue for all superconducting cables is the level of current sharing and stability that is present, these factors are crucially important for large scale applications. Even though the Minimum Quench Energy (MQE) for HTS conductors is much larger than for Low Temperature Superconductors (LTS), current sharing during normal-zone formation resulting from a catastrophic fault-mode is necessary for a more resilient magnet. This work focusses on the stability of one kind of ReBCO cable, the Roebel cable.

Previous stability studies have already been performed on ReBCO tapes, cables, and coils [6,12-19]. The large temperature margins of HTS conductors will likely prevent epoxy cracking, friction from sudden mechanical motion, and flux jumps from initiating a quench [6]. Additionally, the large temperature margin will result in relatively long quench decision times on the order seconds even under adiabatic conditions [15]. Of course, the present requirement for HTS conductor splices in larger coils may introduce some unavoidable heat loads.

The large MQE of HTS cables, especially those operated at 4 K, may make quench unlikely under normal circumstances. However, large-scale systems must be protected under all circumstances. The large MQE makes it much more likely that a fault scenario will be the one that quenches a magnet. Thus, it is important to investigate the stability of a cable under external or fault disturbances as well as normal disturbance generated run-away quench. As will be shown below, this will require consideration not only of the MQE, which assumes short pulses, but also a Minimum Quench Power (MQP) [20]. The MQP concept, originally applied to LTS, will be quite important for HTS tapes, coils, and cables.

This paper is an investigation into the stability properties of non-epoxy impregnated ReBCO Roebel cables. In this paper we start with LN_2 bath-cooled, and under self-field in response to multiple second long heater pulses. A stability diagram was constructed using 77 K experimental and theoretical calculations and a discussion is included to explain the existence of high $i = I/I_c$ (critical current density ratio) standing normal zones. A model is then used to describe distinct types of stability behaviors, including sub-current-sharing excitation, standing normal zone, and slow quench, and an MQP is shown to be a useful parameter in describing cable quench results.

2. Methods

2.1 Roebel cable sample and preparation for measurement

A spool of ReBCO Roebel cable was supplied by W. Goldacker; the parameters describing this cable are listed in table 1, see also [11]. A 380 mm long sample was cut from the spool. Individual tapes were tinned on both top and bottom along a 15 mm length on both ends of the cable. Wood's metal solder was applied with a soldering iron set to a maximum temperature of 130 C°.

2.2 Instrumentation

The Roebel cable was mounted in a shallow channel on a U-shaped G10 glass-phenolic composite holder. The pre-tinned cable ends were soldered onto Cu current leads while they were pressed gently as the Wood's metal cooled. Each side of the U-shaped cable sample was straight approximately 135 mm long. The radius of curvature of the U-shape was 25 mm. A diagram showing the instrumentation on the cable is shown in figure 1.

Voltage taps were soldered onto the surfaces of the tapes for detecting quench propagation. Three Kapton-insulated Nichrome heaters (hot-zone: 4.5 mm width, 3.5 mm length) were attached to tape 3 at the bottom of the U-shape, using 7031 GE-varnish. The first and second heaters were stacked on top of each other and the third backup heater was placed 1 cm horizontally and 0.5 cm longitudinally away. Two Type-E thermocouples were placed on the cable to witness temperature increases from heater pulses and propagation of the hot-zone throughout the cable; one of them was placed on top of the heater stack. After instrumentation, the cable was secured down the legs of the U-shape with Kapton tape, pressing it firmly onto the G-10. The interaction region at the bottom of the U-shape didn't have a layer of Kapton tape and the Roeble cable surfaces were in direct contact with the liquid cryogen bath.

During I_c testing voltage was measured using a Keithley 2182A nanovoltmeter. During stability testing the temperature was measured using a Lakeshore 336 and voltages were measured using a NI-9225 DAQ module. Current was supplied by a stack of HP6634A power supplies. Data were recorded using LabVIEW.

2.3 Measurements

All measurements were taken at self-field in liquid nitrogen, LN_2. For the Roebel geometry, self-field interactions are complex due to interactions between individual tapes and further complicated by the need for a U-shaped sample [21]. At critical current, I_c, the self-field perpendicular to the surface of the cable along the straight sections created by the other straight section was estimated to be less than 0.01 T.

For I_c measurement the cable was slowly cooled in LN_2 and the current was ramped at 1 A/s until quench. The voltage taps measured were V_2 and V_{37}, 36.2 cm apart. Using 10 μV/cm criterion, the cable I_c was 1068 A with an n-value of 15.2.

For stability studies heat pulses of powers ranging from about 1 to 14 W were applied to the cable while it carried reduced currents, i, of 0.75 to 1.17. At the sample, the temperatures sensed by TC_2 and the voltages between tap pairs on tapes 1-9 were recorded.

3. Results

3.1 Critical current of the cable

During I_c measurement a voltage peak was observed at 1100 A after which the cable recovered and continued carrying current beyond its I_c of 1068 A until it quenched at 1130 A. The *I-V* curve is shown in figure 2.

3.2 Cable stability

In response to the heater pulses and *i* values referred to above, three different classes of behavior were observed: no response, stationary normal zone, and slow quench. They are illustrated in figure 3. In the slow quench example, quench protection turned off the current in the middle of the heat pulse.

3.3 Stability phase diagrams

After collecting data for all pairs of *i* and heater powers, diagrams were constructed to represent the three stability regimes. A diagram in the format *i* versus P_{heater}, the power of the heat perturbation, is presented in figure 4.

4. Discussion of the Results

During our measurements, standing normal zones were generated instead of propagating ones. In fact, standing normal zones were witnessed in response to high power heater pulses even at *i* greater than 1.0. While it is true a low power law exponent describing the sharpness of the *I-V* transition to the normal-state, *n*-value, and low I_c criterion contribute to this, the dominant factor is a thermal balance between heat generated from the normal zone and cooling of the sample with the LN_2 -- the basic principle of cryostability.

During the 1960s, 1970s, and early 1980s a great deal of attention was given to the cryostability of LTS conductors immersed in pool boiling LHe. A starting point was the theory of Stekly (e.g. [22] 1968), which provided for the recovery, following a global disturbance, of a superconducting composite operating at its critical current limit. The Stekly parameter $\alpha = G/Q$ described a balance between the ohmic "heat generated", G, by current transferred into the matrix and "cooling", Q, by the boiling cryogen. For $\alpha < 1$, the system is stable and for $\alpha > 1$ the system is unstable and will heat up. A logical extension of Stekly cryostability is the principle of cold-end recovery. As described by Gauster ([23] 1978) and others, if only part of the conductor has quenched, axial heat conduction to the part that is still at bath temperature will enable a return to the superconducting state. Cold-end recovery was well described geometrically by the equal-area theorem of Maddock, James, and Norris ([24] 1969]. Then in extensions of this description Meuris ([25] 1981) and Dresner ([26] 1982) considered the conditions under which a conductor can remain in stable thermal equilibrium in the presence of a permanent source of extra localized heat generation or disturbance, G_d.

4.1 Stekly Cryostability

Transferring the above principals of cryostability from LTS to HTS lead to some surprising results that stem principally from: (i) differences between the heat transfer coefficients of surfaces, h, in pool boiling He and those in pool boiling LN_2, (ii) the differences in Stabilizer/Superconductor ratio which in ReBCO is typically 40:1 [27] to 60:1 [28]. In performing the following analyses, we made use of the pool-boiling data of Kida et al [29]. Based on their figure 2 we produced tables of the change in temperature from the liquid cryogen, ΔT, and the cooling power normalized to the conductor surface area, Q. Because $h = Q/\Delta T$, we were able to create functions of h versus ΔT for nucleate and film boiling, respectively, of the forms

$$h = 0.6953 + 0.001079 \times \Delta T^4 \qquad (\Delta T = 2\text{-}11\ \text{K}) \qquad \text{kW/m}^2\text{K} \quad \text{(nucleate)} \qquad (1)$$

$$h = \frac{(a+b\times\Delta T)}{(1+c\times\Delta T)} \quad \text{where} \quad \begin{matrix} a = -5.787 \\ b = -0.155 \\ c = -0.546 \end{matrix} \qquad (\Delta T = 8\text{-}300\ \text{K}) \qquad \text{kW/m}^2\text{K} \quad \text{(film)} \qquad (2)$$

To begin, Stekly analysis was applied to a model stack of nine ReBCO tapes. Considering a cable which was not epoxy impregnated, we accounted for heat removal from the total tape surface within the cable; in this case it was useful to define a total tape perimeter in a cross section, P = 9 x the tape perimeter (11.4 mm) = 102.6 mm. Referring to table 2, we calculated the ohmic heat generated in the tapes' Cu stabilizer (resistance R) by the transferred critical current I_c. This is $G = I_c^2R = I_c^2\rho L/A_{Cu}$, where A_{Cu} is the transverse area of the stabilizer. This G, normalized to unit length and unit total strand-surface area (PL) is

$$G = \frac{\rho I_c^2}{PA_{Cu}} = 5.49\ \text{kW/m}^2 \qquad (3)$$

This we compared with the surface cooling power $Q = h(T\text{-}T_b) = h\Delta T$ where T_b is the bath temperature (77 K). According to [29] the maximum cooling power of nucleate boiling LN_2 is

$$Q_{max} = 200\ \text{kW/m}^2 \qquad (4)$$

Based on eqns (3) and (4) we find for the Stekly parameter

$$\alpha = G/Q_{max} = 0.027 \qquad (5)$$

Thus, with an $\alpha \ll 1$, the cable far exceeds the Stekly limit for cryostability. In equilibrium ($G = Q = h\Delta T$), while supporting a power generation of 5.49 kW/m^2, the ΔT of the stack (based on eqn (1)) would not exceed 4.5 K (T_{stack} = 81.5 K).

On the Stekly basis, the cable would continue to be stable against a disturbance of 194 kW/m^2. The Stekly criterion assumes instantaneous and spatial homogenization of all cooling and heating

power; this isn't realistic to cryogen bath cooled systems and certainly not in epoxy impregnated systems. In reality such disturbances, when externally applied over a given length, may cause the cooling to locally transition to film boiling, lower the margin of stability, and may remove the cable from the Stekly stable regime. To describe this condition, we modified the Stekly heat-generation/cooling balance to include an external heat perturbation, one that might originate from a localized fault.

4.2 Extra Heat Generation from a Fault

Adding a fault or generalized disturbance, G_d (per unit length and total tape surface area, A_s), the total heat generated per unit length is now

$$G' = \frac{\rho I_c^2}{PA_{Cu}} + G_d \qquad \text{W/m}^2 \qquad (6)$$

Using $Q = h(T\text{-}T_b)$, this leads to

$$\alpha' = \frac{\frac{\rho I_c^2}{PA_{Cu}} + G_d}{h(T\text{-}T_b)} \qquad (7)$$

If $\alpha' < 1$, the sample is always cooling towards the bath temperature. If $\alpha' > 1$, the sample temperature will rise, and if $\alpha' = 1$, an equilibrium is established at some $T > T_b$, given by

$$\Delta T = T\text{-}T_b = \frac{\frac{\rho I_c^2}{PA_{Cu}} + G_d}{h} \qquad (8)$$

This predicts that a cable with a certain current applied and a certain heat perturbation will increase in temperature until a stable point is reached.

In the present experiment, heat perturbations were created with a heating element (see table 2 for details). With 10 W applied, initially only the surface of the top tape under the heater with an area, A_Z = 4.5 x 3.5 mm, would be active. Therefore, $G_{d(t=0)} = 10/A_Z = 634.9$ kW/m^2 and $G + G_{d(t=0)} = 640.4$ kW/m^2. This would put the tape into the film boiling regime where it would

remain as the heat fully permeates the whole stack. Then assuming power deposition and cryogenic cooling on all tape surfaces (see table 2) the cable stack's local G_d would drop to $G_d/A_s = 35.27$ kW/m^2 (with $G + G_d = 40.76$ kW/m^2) which based on eqn (8) provides a ΔT_{film} of 104 K. The theoretical 181 K normal zone would recover to the superconducting state when the heater is switched off.

According to the Stekly model, with a disturbance margin ($Q_{max} - G$) of ~190 kW/m^2 ohmically generated internally, the cable is super cryostable. But it is much less stable with respect to an externally applied disturbance which quickly initiates film boiling. Analysis using eqn (8) shows that a surface-applied G_d as small as 11 kW/m^2 would be sufficient to drive the current-carrying cable normal.

4.3 Cold-End Cooling

In addition to the direct cryogenic cooling of the heated zone taking place at a rate $h\Delta T$ heat is also being heat removed by conduction along the cable. This "cold-end cooling", Q_{ce}, takes place at a rate

$$Q_{ce} = 2\frac{\kappa A_{Cu}\,\Delta T}{X_c} \qquad \text{W} \qquad (9)$$

which represents heat transport down a linear temperature gradient $\Delta T/X_c$. X_c is the distance over which the cable temperature drops from T to T_b, and the factor 2 accounts for cooling to both ends of the cable. Recognizing that this heat was being deposited from both ends of the hot zone into the cryogen bath via pool boiling LN_2 at a rate $Q_{ce} = 2X_cPh(\Delta T/2)$ (where $\Delta T/2$ is the average of T

and T_b) and equating these two forms of Q_{ce}, it is clear $X_c = \sqrt{2\kappa A_{Cu}/Ph}$. Substitution of this into eqn (9) yields

$$Q_{ce} = T\sqrt{2\kappa A_{Cu} Ph} \qquad \text{W} \qquad (10)$$

Normalized to A_s, the surface area of all the tapes in the event zone (table 2), this becomes

$$Q_{ce}'' = \frac{\Delta T\sqrt{2\kappa A_{Cu} Ph}}{A_s} \qquad \text{W/m}^2 \qquad (11)$$

So that the total cooling becomes

$$Q'' = \eta h \Delta T + \frac{\Delta T\sqrt{2\eta\kappa A_{Cu} Ph}}{A_s} \qquad \text{W/m}^2 \qquad (12)$$

in which we have introduced an "efficiency factor", η, to recognize that not all the tape surfaces are exposed to the liquid cryogen. The heat-balance equation for cold-end cooling is then

$$1 = \frac{G + G_d}{\eta h \Delta T + \frac{\Delta T\sqrt{2\eta\kappa A_{Cu} Ph}}{A_s}} \qquad (13)$$

such that

$$\Delta T = \frac{\frac{\rho I_c^2}{PA_{Cu}} + G_d}{\eta h + \frac{\sqrt{2\kappa A_{Cu} P\eta h}}{A_s}} \qquad (14)$$

which after values (based on Ws *not* kWs) from the above and temperature independent properties in table 2 have been inserted becomes

$$\Delta T = \frac{40.76\times10^3}{\eta h + 72.06\sqrt{\eta h}} \qquad (15)$$

Eqn (15) can be thought of as representing h as function of ΔT for a set of η values which could range from 0.25 (low cooling efficiency) to 1 (in which all tape surfaces receive cooling). Since film boiling was expected, h versus ΔT must also satisfy eqn (2). The points of intersection of these two $h(\Delta T)$ curves, one from the group constructed from various chosen values of η in eqn (15) and the other for film boiling in eqn (2), are shown in figure 5. Some representative values are listed in table 3. Worth noting is the introduction of cold-end cooling reduced ΔT from 104 K to 10~38 K depending on the cooling efficiency. Experimentally we measured a ΔT of 31 K (figure 5) which indicates in this case a cooling efficiency of $\eta = 0.31$.

4.4 Comparison of Theory and Experiment

Based on eqn (14) it was possible to plot ΔT versus G_d for a range of values of reduced transport current. In our analysis we assumed a $T_c = 91$ K, a temperature dependent I_c of the form

$$I_c\,(T<T_c) = I_c(77\text{ K})\frac{T_c-T}{T_c-77} \tag{16}$$

and a temperature dependent ρ of the form

$$\rho(T) = \rho(273\text{ K}) - 7\times10^{-11}(273\text{ K} - T) \qquad \Omega\text{m} \tag{17}$$

Additionally, we allowed for current sharing rather than a sharp transition to fully normal state current by replacing the I_c implicit in eqn (14) by $(I - I_c)$. The analytical predictions are compared with the experimental results in figure 6.

There is no noticeable influence of i on either the experimental or the theoretical values of ΔT because the numerator of eqn (14) is dominated by the second term, G_d. Under these experimental conditions (pool boiling LN_2 with cryogen infiltration into the cable) the cable was well cooled

with respect to the level of heat generated by current flow, even in the normal state. Because of the weak influence of i, the expected curvature resulting from current sharing and a temperature dependent I_c is not seen. For the same reason, the $i = 0.66$ and $i = 0.84$ curves strongly overlap. A comparison of the experimental and theoretical curves shows reasonable agreement over much of the input power range. However, no obvious transition from nucleate to film boiling is seen in the experimental data. Indeed, near the expected transition is where the largest discrepancy between experiment and theory is seen. This may be explained because this simple theoretical model assumes an sharp transition from nucleate to film boiling while in reality a mixed boiling regime will exist across the temperature gradient and a more advanced analysis similar to that performed by Breschi et al. for LHe will provide a more realistic picture near this discrepancy [30]. Nevertheless, the model clearly demonstrates (i) the existence of three distinct types of stability behaviors (sub-current-sharing excitation, standing normal zone, slow quench), (ii) the importance of cooling efficiency (coolant penetration into the stack), (iii) the susceptibility of HTS cables to external disturbances, because of the tendency to transition to the film boiling regime at the earliest times of the excitation, and (iv) the importance of minimum cooling power in describing cable quench results. These measurements were performed in LN_2, but the procedure presented in this paper is also suitable for analyzing stability under LHe bath cooling.

5. Summary

Stability responses for variable i and heater pulses were plotted for a 9/5.6 ReBCO Roebel cable at 77 K and self-field to create stability phase diagrams. Three distinct types of stability behaviors were created: sub-current-sharing excitation, standing normal zone, and slow quench. Fast quench, while not described here, would require a heat capacity term as well other considerations. The

stability behavior was initially described using a modified Stekly criterion. It was pointed out that the heat generated (G~6 kW/m^2) by I_c transfer to the Cu matrix was very much less than the maximum nucleate boiling cooling by LN_2 (Q = 200 kW/m^2). Thus, with a Stekly parameter $\alpha = G/Q$ « 1 and a heat generation margin of ~190 kW/m^2 the present Roebel ReBCO cable was shown, assuming direct contact with liquid cryogen, to be ultra-cryostable with respect to internally generated transport current overload. Not so to an externally applied disturbance, G_d. Locally applied heat of only 35 kW/m^2 was found sufficient to drive the cryogen into film boiling and to raise a normal zone's temperature to 181 K. In practice, however, the normal zone receives extra cooling by conduction to both ends of the LN_2 immersed cable. The introduction of this "cold-end cooling" lowered the zone temperature to 87 K. Based on calculations that included both the extra localized heat generation, G_d, and the cold-end cooling a set of curves was generated to enable the estimation of normal zone temperature (77 K + ΔT) as a function of cryogenic cooling efficiency. Comparing this to our experimental results (31 K for a 10 W surface disturbance) led to the determination of an efficiency factor of η = 0.31. A model was used which showed the existence of three distinct types of stability behaviors (sub-current-sharing excitation, standing normal zone, slow quench). In addition, it quantified the importance of cooling efficiency. Lastly, it described the importance of minimum cooling power in describing cable quench results.

Acknowledgements

Funding was provided by the U.S. Department of Energy, Office of High Energy Physics, under Grant DE-SC0011721.

References

[1] van Nugteren, J 2016 ‘High Temperature Superconductor Accelerator Magnets’, PhD thesis, University of Twente, The Netherlands.

[2] Weijers, HW 2009 ‘High-Temperature Superconductors in High Field Magnets’, PhD thesis, University of Twente, The Netherlands.

[3] Qu T, Michael PC, Bascunan J, Lecrevisse T, Guan M, Hahn S, and Iwasa Y 2017, ‘Test of an 8.66-T REBCO insert coil with overbanding radial build for a 1.3 GHz LTS/HTS NMR magnet’, *IEEE Trans. Appl. Supercond.*, vol. 27, no. 4, Art no. 4600605.

[4] Breschi M, Cavallucci L, Ribani PL, Gavrilin AV, and Weijers HW 2017, ‘Modeling of quench in the coupled HTS insert/LTS outsert magnet system of the NHMFL’, *IEEE Trans. Appl. Supercond.*, vol. 27, no. 5, Art no. 4301013.

[5] http://www.businesswire.com/news/home/20150917005142/en/

[6] Kirby GA *et al.* 2017, ‘First cold powering test of REBCO Roebel wound coil for the EuCARD2 future magnet development project’, *IEEE Trans. Appl. Supercond.*, vol. 27, no. 4, Art no. 4003307.

[7] Godeke A *et al.* 2017, ‘A feasibility study of high-strength Bi-2223 conductor for high-field solenoids’, *SUST*, vol. 30, Art no. 035011.

[8] Bayer CM, Gade PV, Barth C, Preub A, Jung A and Weib KP 2016, ‘Mechanical reinforcement for RACC cables in high magnetic background fields’, *SUST*, vol. 29, Art no. 025007.

[9] Talantsev EF, Badcock RA, Mataira R, Chong SV, Bouloukakis K, Hamilton K and Long NJ 2017, ‘Critical current retention of potted and unpotted REBCO Roebel cables under transverse pressure and thermal cycling’, *SUST*, vol. 30, Art no. 045014.

[10] Bayer, C 2013 'High Temperature Superconductor Cable Concepts for Fusion Magnets', PhD Thesis, Karlsruher Institute of Technology, Karlsruhe, Baden Wurttemberg, Germany.

[11] Long NJ, Badcock RA, Hamilton K, Wright A, Jiang Z and Lakshmi LS 2010, 'Development of YBCO Roebel cables for high current transport and low AC loss applications', *Journal of Physics: Conference Series*, vol. 234, Art no. 022021.

[12] Murphy JP *et al.* 2013, 'Experiment setup for Calorimetric measurements of losses in HTS coils due to AC current and external magnetic fields', *IEEE Trans. Appl. Supercond.*, vol. 23, no. 3, Art no. 4701505.

[13] Levin GA, Barnes PN, Rodriguez JP, Connors JA, and Bulmer JS 2009, 'Stability and normal zone propagation speed in YBCO coated conductors with increased interfacial resistance', *IEEE Trans. Appl. Supercond.*, vol. 19, no. 3, pp.2504-2507.

[14] Duckworth RC, Pfotenhauer JM, Lue JW, Gouge MJ, Lee DF, and Kroeger DM 2002, 'Quench dynamics in Silver coated YBCO tapes', *Adv. Cryog. Eng.*, vol. 47, pp.449-456.

[15] Song H and Schwartz J 2009, 'Stability and quench behavior of $YBa_2Cu_3O_{7-x}$ coated conductor at 4.2 K, self-field', *IEEE Trans. Appl. Supercond.*, vol. 19, no. 5, pp. 3735-43.

[16] Ishiyama A *et al.* 2005, 'Normal transition and propagation characteristics of YBCO tape', *IEEE Trans. Appl. Supercond.*, vol. 15, no. 2, pp.1659-1662.

[17] Ishiyama A, Tsuchiya M, Ueda H and Shiohara Y 2007, 'Assessment of cryogenic thermography system using commercial fluorescent paints on their applicability to

visualization of normal-zone propagation in YBCO coated conductor', *IEEE Trans. Appl. Supercond.*, vol. 17, no. 2, pp.3765-3768.

[18] Angurel LA *et al.* 2009, 'Analysis of quench initiation in YBCO coated conductors using optical interferometric techniques', *IEEE Trans. Appl. Supercond.*, vol. 19, no. 3, pp.3479-3482.

[19] Haro E, Stenvall A, van Nugteren J and Kirby G 2015, 'Modeling of minimum energy required to quench an HTS magnet with a strip heater', *IEEE Trans. Appl. Supercond.*, vol. 25, no. 6, Art no. 4701505.

[20] Awaji S, Hou Y, Oguro H, Watanabe K, Inoue I, Sakamoto H, Yasumaga S and Ryu J 2012, 'Hot spot behavior of Y123 coated conductors', *IEEE Trans. Appl. Supercond.*, vol. 22, no. 3, Art no. 6601004.

[21] Goldacker W, Frank A, Kudymow A, Heller R, Kling A, Terzieva S and Schmidt C 2009, 'Status of high transport current Roebel assembled coated conductor cables', *SUST*, vol. 22, Art no. 034003.

[22] Stekly ZJJ, Thome R, and Strauss B 1968, 'Principles of stability in cooled superconducting magnets', in *Proc. Summer Study on Superconducting Devices and Accelerators*, ed. J.P. Blewett et al., Brookhaven National Laboratory, pp. 748-764

[23] Gauster WF 1978 'A note on the cryostatic stability of superconducting composites', *Report No. ORNL/TM-5989*, to the Fusion Energy Division, Dept. of Energy, from Oak Ridge National Laboratory, TN.

[24] Maddock BJ, James GB, and Norris WT 1969, 'Superconductive composites: heat transfer and steady state stabilization', *Cryogenics*, vol. 9, pp. 261-273.

[25] Meuris C 1981 ‘Influence of an uncooled region on the stability of superconducting conductors’, in *Stability of Superconductors in Helium I and Helium II*, Int. Inst. of Refrig., Paris, pp. 161-168.

[26] Dresner L 1982, ‘Maximum allowable resistive zone in a metastable superconductor’, *Report No. ORNL/TM-8394*, to the Fusion Energy Division, Dept. of Energy, from Oak Ridge National Laboratory, TN.

[27] http://www.superpower- inc.com/system/files/SP_2G+Wire+Spec+Sheet

[28] http://www.superpower-inc.com/content/2g-hts-wire

[29] Kida M, Kikuchi Y, Takahashi O and Michiyoshi I 1981, ‘Pool-Boiling Heat Transfer in Liquid Nitrogen’, *J. Nucl. Sci. Technolog*y, vol. 18, no. 7, pp. 501-503.

[30] Breschi M, Trevisani L, Bottura L, Devred A, and Trillaud L 2008, ‘Comparing Thermal Stability of NbTi and Nb_3Sn Wires’, *Departmental Report CERN/AT 2008-28*, to the European Organization for Nuclear Research, Laboratory for Particle Physics

List of Tables

Table 1. ReBCO Roebel cable parameters.

Parameter	Specification
Roebel cable manufacturer	Karlsruhe Institute of Technology
ReBCO tape manufacturer	SuperPower Inc.
Type of Roebel cable	9/5.6
Number of Tapes	9
Tape Width, w_{tape} (mm)	5.6
Cable Width, W_C (mm)	11.8
Insulation	3-layers of Kapton over cable (not individual tapes). No epoxy impregnation.
Tape thickness, t_{tape} (mm)	0.1
Pitch Length, L_p (mm)	126
Cross-over angle, ϕ (degrees)	40
$L_{Inter\text{-}strand\ gap}$ (mm)	0.4
$W_{Cross\text{-}over}$ (mm)	5.6
I_c @ 77 K, sum of tapes (A)	1168

Table 2. Parameters for Stability Analysis

Tape width, w_{tape}	= 5.6 mm
Cable (9-tape) perimeter, P = 9 x 2 x (w_{tape}+t_{tape})	= 103.5 mm
ReBCO layer thickness, t_{SC}	= 1.6 μm
Cu layer thickness, t_{Cu}, = 2 x 50 μm	= 0.1 mm
Cable (9-tape) Cu c/s area, A_{Cu} = 9 x w_{tape} x t_{Cu}	= 5.04 mm^2
Cu resistivity at 77 K, ρ	= 2.1 x 10^{-9} Ωm
Cable critical current at 77 K, I_c	= 1.168 kA
Heater length, H_l	= 3.5 mm
Heater width, H_w	= 4.5 mm
Heater surface area, $A_H = H_l$ x H_w	= 1.575 x 10^{-5} m^2
Top surface area of one tape in the event zone, $A_z = A_H$	= 1.575 x 10^{-5} m^2
Surface area of all tapes in the event zone, $A_s = A_z$ x2 x 9	= 2.835 x 10^{-4} m^2
Heat perturbation at 10 W, $G_d = 10/A_s$	= 3.527 x 10^4 W/m^2
Cable thermal conductivity, κ,	= 400 W/mK

Table 3. Influence of cooling efficiency on the response to a localized surface disturbance of 10 W under cold-end cooling

η	h, W/m^{2}K	ΔT, K
0.25	602	38.1
0.4	808	24.4
0.5	971	19.2
0.8	1710	10.0

List of Figures

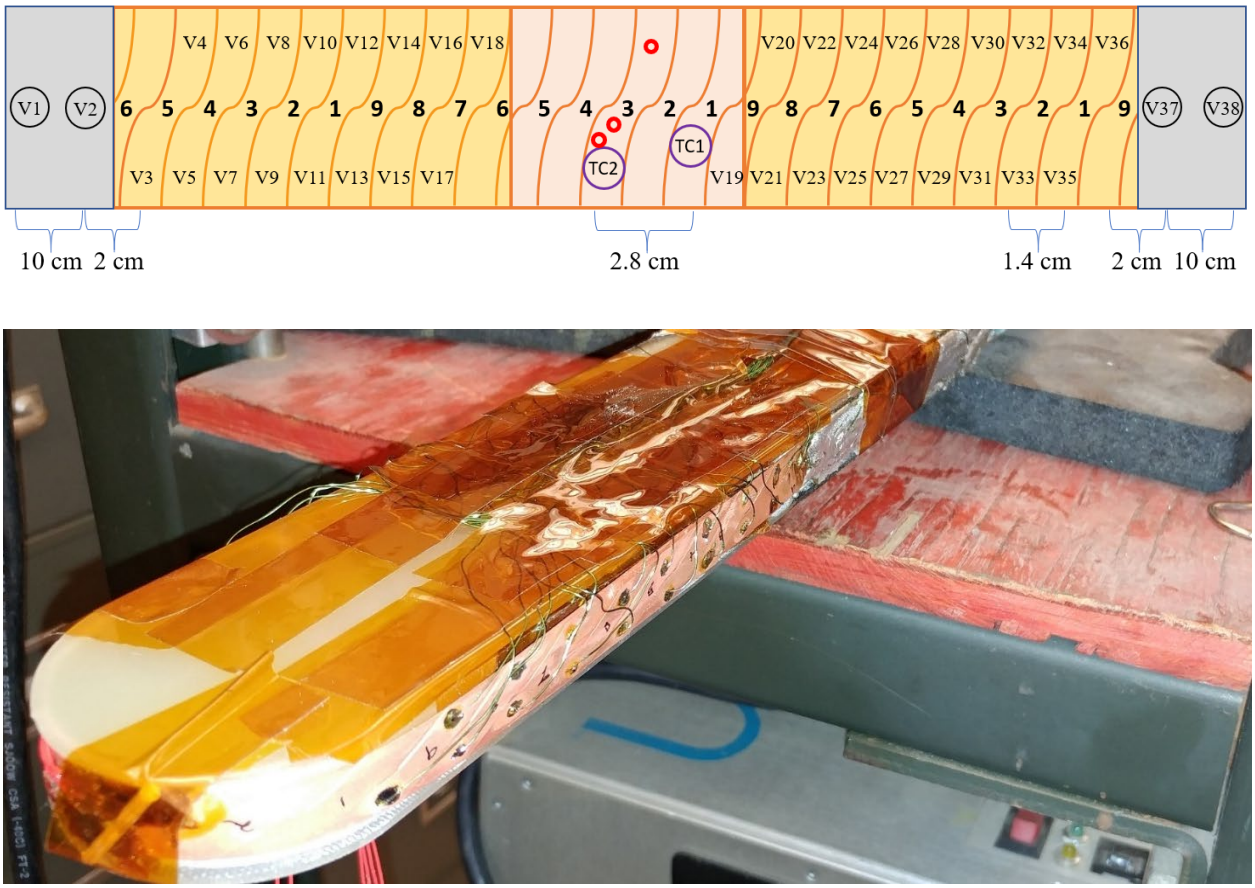

Figure 1. (Top) Instrumentation diagram of the 9/5.6 ReBCO Roebel cable on the U-shaped G10 holder. The silver areas are the 15 cm soldered regions of the cable on the Cu current leads, the golden areas are where the sample has a layer of Kapton tape, and the Copper colored area is the uncovered interaction region. The V#s are location of the voltage taps, the red circles are the location of the 40 Ω Kapton/Nichrome heaters, and the and the purple numbered circles, TC1 and TC2, are the locations of the Type-E thermocouples. The tape numbers, 1-9, are shown in bold. (Bottom) image of V_{19} to V_{38} before being covered with a layer of Kapton tape and heaters mounted on the sample. The layer of Kapton tape on the bottom of the U-shaped holder over the heaters was removed during sample measurement.

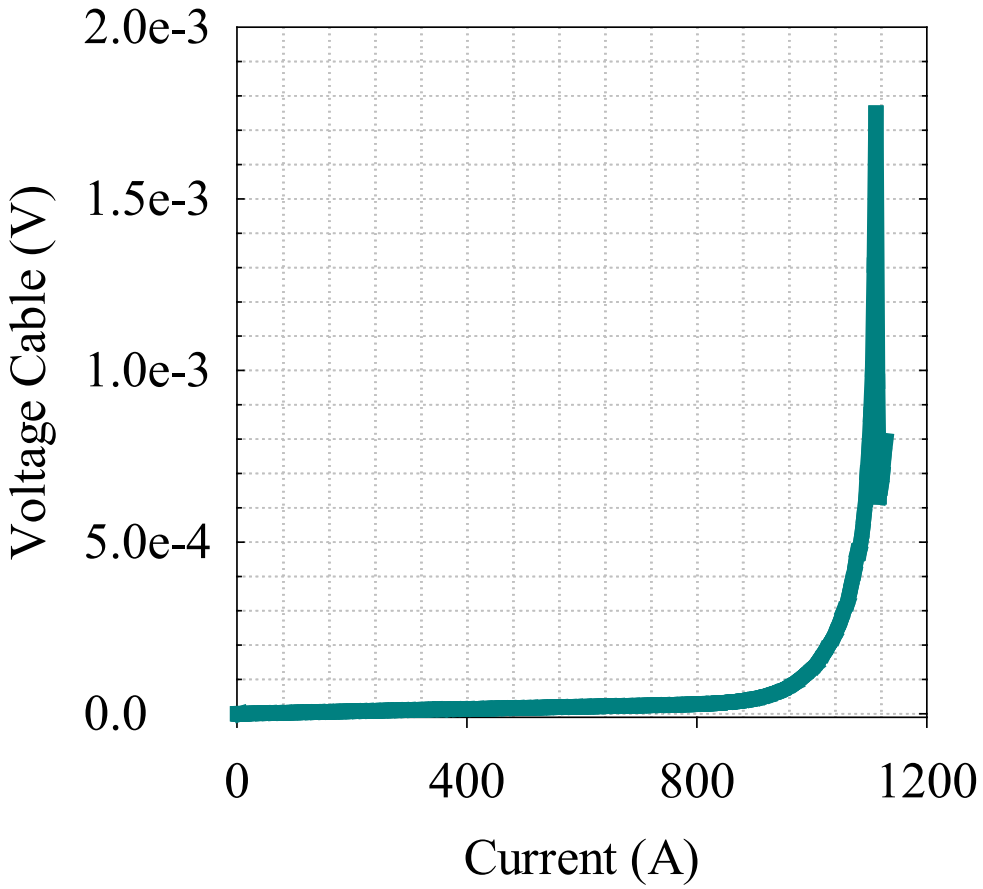

Figure 2. *I-V* data at 77 K and self-field for ReBCO Roebel cable. The I_c was 1068 A, the *n*-value was 15.2, and I_q was 1130 A.

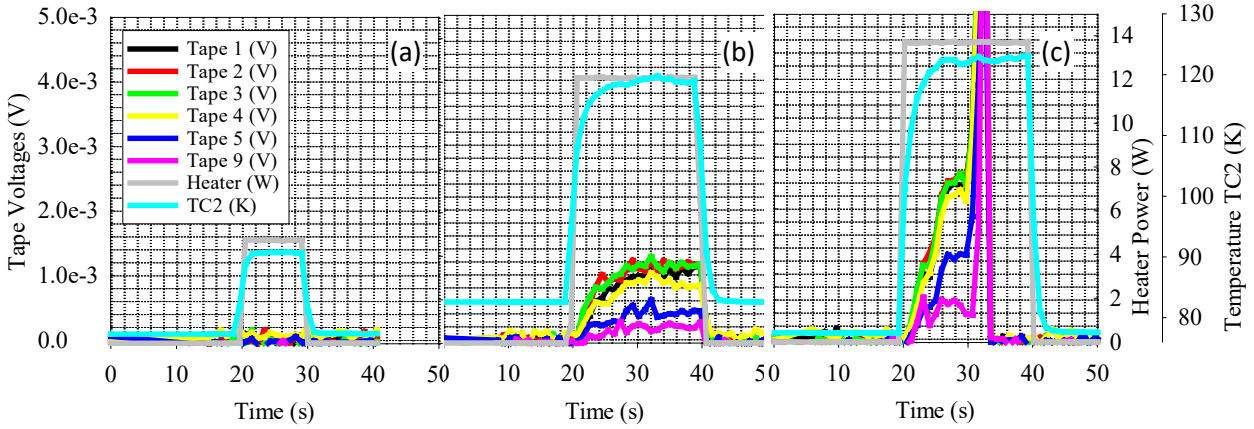

Figure 3. Three classes of stability response to heat pulses at various i: (a) no response: $i = 0.9348$, $P_{heater} = 4.8$ W, $E_{heater} = 48$ J (b) stationary normal zone: $i = 0.9615$, $P_{heater} = 12.3$ W, $E_{heater} = 246$ J, (c) slow quench: $i = 0.9615$, $P_{heater} = 13.9$ W, $E_{heater} = 277$ J.

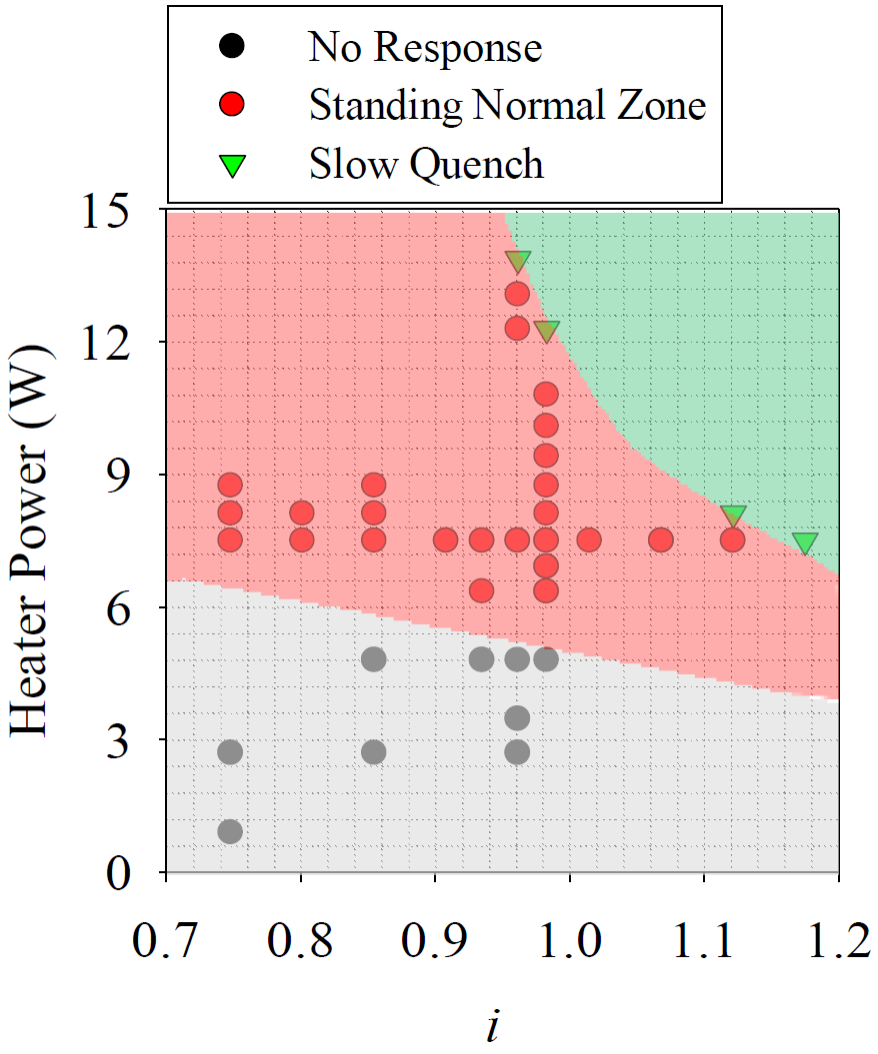

Figure 4. Stability diagram of observed stability responses for variable *i* versus heater power. Arbitrary boundaries were created to make regions of stability response more visible.

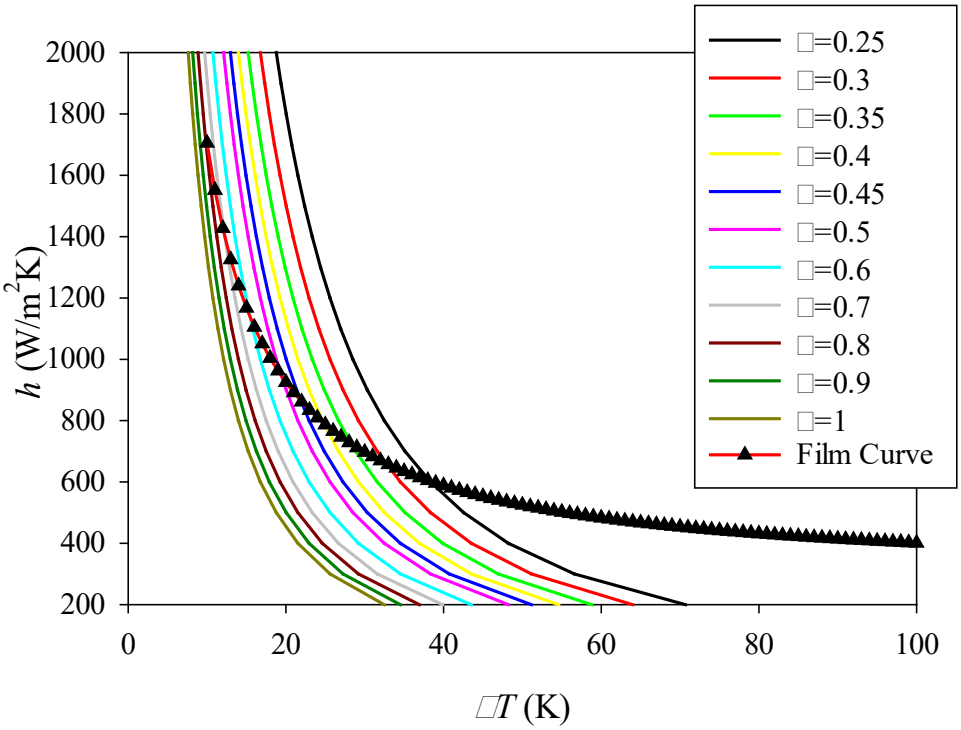

Figure 5. Film boiling h (W/m^{2}K) versus ΔT based on eqn (2) (points) and eqn (15) plotted for η-values of 0.25 to 1 (continuous lines). Some points of intersection are listed in table 3.

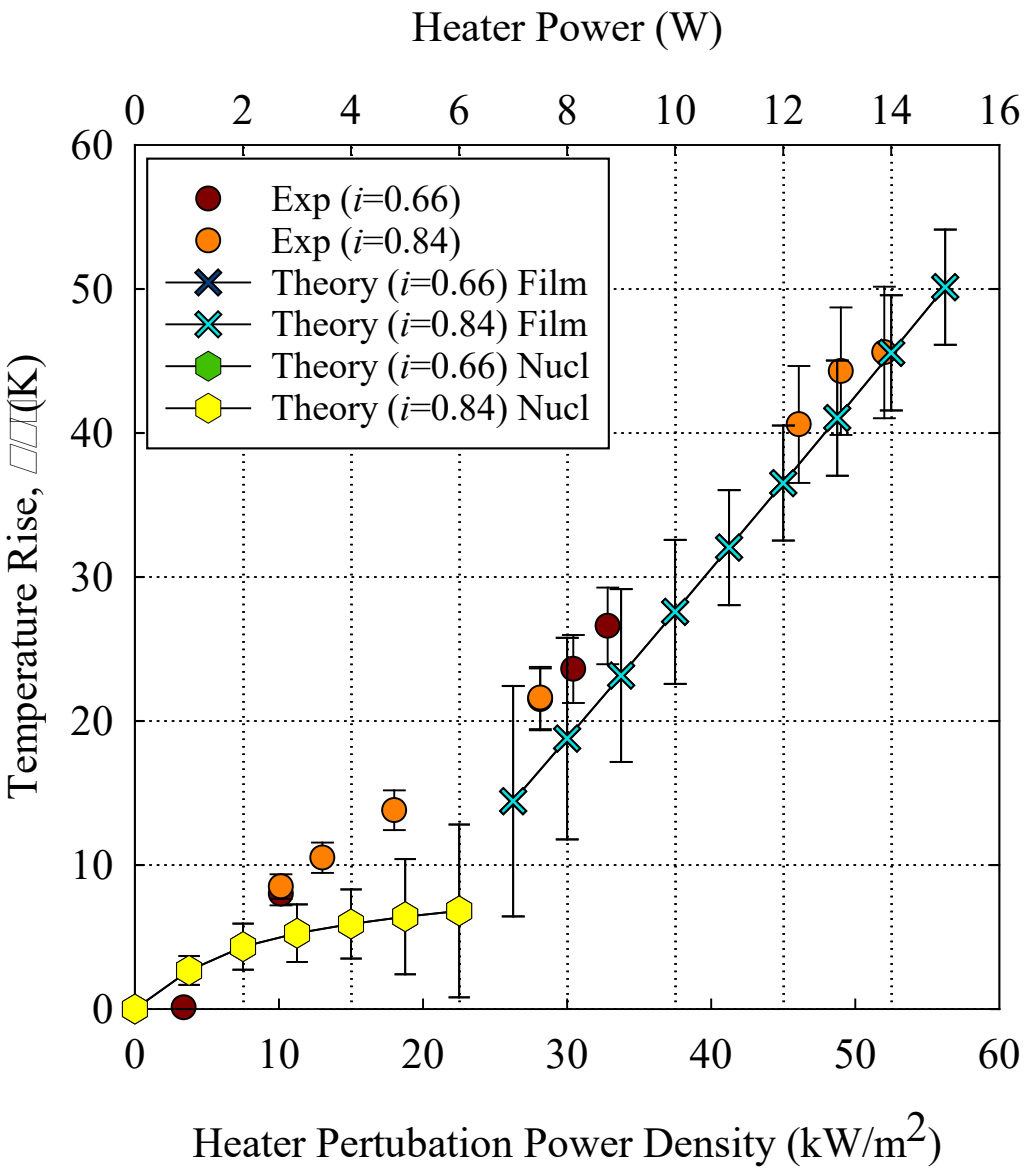

Figure 6. ΔT as function of G_d: experimental results compared with theory, eqn (14,16,17).